Phase stability of wüstite at high pressure from first-principles linearized augmented plane-wave calculations

Donald G. Isaak*
Institute for Geophysics and Planetary Physics, University of California, Los Angeles, California 90024-1567

Ronald E. Cohen
Geophysical Laboratory and Center for High Pressure Research, Carnegie Institution of Washington, Washington, District of Columbia 20015-1305

Michael J. Mehl and David J. Singh
Complex Systems Theory Branch, Naval Research Laboratory, Washington, District of Columbia 20375-5000
(Received 1 September 1992)

We use the local spin-density approximation (LSDA) to investigate the phase stability and physical properties of stoichiometric wüstite at high pressure. Highly converged total-energy calculations are presented for nonmagnetic, ferromagnetic, and antiferromagnetic, unstrained $B1$ and $B2$, and rhombohedrally strained $B1$ structures. We find the local magnetic moments are greatly diminished at high pressure, and we expect the LSDA to provide an accurate description of FeO at high pressure. The antiferromagnetic ground state occurs for a small rhombohedral distortion of the $B1$ structure. The rhombohedral angle α decreases with increasing pressure, in agreement with available x-ray data. Our results elucidate the phase relationship between the $B1$ and $B2$ structures of FeO, and explain why no transition has yet been observed in room-temperature static experiments up to 220 GPa, whereas a transition to a metallic, and possibly $B2$, phase has been observed at 70 GPa and high temperature. We predict that a transition to a metallic $B2$ structure will occur from a rhombohedrally strained $B1$ metallic phase near 500 GPa, provided no further distortions to lower symmetry occur in the rhombohedral lattice.

I. INTRODUCTION

Among the transition-metal monoxides, MnO, FeO, CoO, and NiO, Fe_xO (the mineral wüstite) has particular importance because it is an end member of magnesiowüstite $Mg_yFe_{1-y}O$ which is likely to exist in the Earth's deep interior.[1] Despite considerable study by both high-pressure experiments and theoretical first-principles methods, many questions persist regarding the nature of the bonding, and the electrical, magnetic, and structural properties of FeO at high pressure. Experimentally, wüstite is also complicated by nonstoichiometry and local defect clusters[2] which we do not consider here; all of our calculations are for stoichiometric FeO.

At ambient pressure and temperature FeO is paramagnetic (PM) with disordered local moments on the Fe^{2+} ions. An antiferromagnetic (AFM), rhombohedral distorted $B1$ phase (stretching along a body diagonal of the rocksalt cell) is observed experimentally when temperature is decreased below the Néel temperature $T_N \approx 198$ K at ambient pressure.[3,4] Neutron diffraction studies[5] show that the AFM ordering is such that Fe^{2+} ions in planes perpendicular to the (111) direction all have parallel spins, and the spins between adjacent planes are antiparallel. The rhombohedral angle α is 59.4° for $Fe_{0.97}O$ at 90 K and ambient pressure,[4] compared to 60° for the undistorted cubic $B1$ structure.

X-ray data obtained *in situ* with diamond anvil experiments at room temperature and pressures up to 70 GPa,[6] 70 GPa,[44] 120 GPa,[7] and 220 GPa (Ref. 45) all indicate no evidence of a first-order phase transition with a significant change in volume. Zou *et al.*[6] found that the (111) x-ray diffractions begin to broaden at 9 GPa, and around 25 GPa are resolved to split into two lines, (003) and (101), consistent with a rhombohedral distortion. The resolution of a broad Fe-Mössbauer spectra into a six-peak hyperfine structure[6] supports the interpretation of a rhombohedral cell at elevated pressure. Yagi, Suzuki, and Akimoto[7] were able to resolve a splitting of the (111) peaks at 16 GPa when using a pressure medium and note that the sharpness of the transition is quite sensitive to the pressure environment. For their sample with $x = 0.98$, they found at 20 GPa that $\alpha = 57.5°$. Both Zou *et al.*[6] and Yagi, Susuki, and Akimoto[7] infer that the rhombohedral distortion is coincident with a paramagnetic to antiferromagnetic transition as T_N is crossed at elevated pressure. Apparently T_N tends to increase with increasing pressure in the pressure range 0–26 GPa.

As pressure is increased above the PM-AFM transition at room temperature, the x-ray data indicate that the rhombohedral distortions tend to increase.[6,7] However, at pressures greater than 30 GPa the difference between a particular observed d line and that calculated with a least squares fit using multiple d lines is larger than the experi-

mental uncertainty, making an interpretation of the x-ray data in terms of a rhombohedral cell at these pressure less certain. Yagi *et al.*[7] note problems in maintaining hydrostatic conditions due to the solidification of their pressure medium (methanol-alcohol). They point to the preferential orientation of the elongated body diagonal perpendicular to both the uniaxial stress direction of the diamond cell and to the direction of the incident x-ray beam as possible explanations for the disagreement between the calculated and observed d spacing, as well as the variations in line intensities, for $P \geq 30$ GPa. The further splitting of the (220) peak just below 40 GPa suggests that further distortions from the rhombohedral cell to lower symmetry may also occur. These line intensities are very weak, however, and may be caused by nonhydrostatic conditions in the diamond cell.

In contrast with the static high-pressure data at room temperature, shock studies show evidence for a phase transition; at 70 GPa on the shock Hugoniot there is a marked resistivity change accompanied by a 4% decrease in volume.[8–11] The shock data are quite reproducible in spite of a range of stoichiometric and porosity conditions for the samples. Knittle and Jeanlog[12] measured the temperature and pressure dependence of the resistivity ρ of $Fe_{0.94}O$ in a diamond cell. They found no significant change in ρ at room temperature over the pressure range 0–83 GPa. However, at pressures greater than 70 GPa they found metallization occurs when heating to temperatures greater than about 1000 K, but not when the heat was applied at pressures less than about 70 GPa. The conclusion of Knittle and Jeanloz[12] is that at simultaneous pressure and temperatures above 70 GPa and 1000 K, respectively, a metallic phase occurs. They[12] infer (see their Fig. 8) that the boundary between the metallic and insulating phases is approximately independent of temperature above 1000 K.

Whether or not this insulating to metallic transition is accompanied by a structural change is uncertain,[9,12] and is an important question to resolve since an accurate description of the chemical, thermal, and magnetic processes in the deep Earth require this information.[13] Jeanloz and Ahrens[8] infer that the volume change observed at 70 GPa on the shock Hugoiniot represents a $B1$ to $B2$ (CsCl) structural transition, while others have suggested a transition to the $B8$ (NiAs) structure.[14] However, the discontinuous change in volume at 70 GPa on the Hugoniot may also be in response to an isostructural collapse of the lattice at the onset of metallization.[12,15–18] Though no consensus exists on the precise nature of the 70 GPa transition at high-temperature, it is apparent that an FeO phase exists at simultaneous elevated pressure and temperature which has not been identified to date in high pressure experiments at low temperature.

We use the local spin-density approximation (LSDA) to study the high-pressure properties of stoichiometric FeO. These calculations were done using the linearized augmented plane-wave (LAPW) method. We calculate total energies of FeO over the range in volumes $9 - 21$ Å^3 for the primitive cell, and consider both $B1$ and $B2$ lattice structures, as well as rhombohedral strains of the $B1$ lattice. Our calculations are done for the cases of nonmagnetic (NM) FeO (i.e., no local moments, or "low spin" Fe^{2+}), and both ferromagnetic (FM) and AFM spin ordering. We wish to address what effect pressure has on the magnitude of the static structural and magnetic phases of stoichiometric FeO, with the view to better understand the bonding in FeO at high pressure and temperature, and the nature of the metallic high-pressure phase.

It is well documented that the ground state properties of FeO and other transition-metal monoxides are not completely described by theoretical band calculations using the LSDA. A model for self-consistently including the local correlations in a density functional calculation[19] is very promising but it is not yet computationally feasible to study the metal-insulator transition in FeO using such methods at the present time. In spite of the inability of the LSDA to correctly predict the insulating character of FeO at zero pressure, we believe that the LSDA gives reasonably accurate total energies, and that this is especially true at high pressure since the problems in the ground states of the transition-metal monoxides at ambient pressure are most likely related to the magnetic moments of the metal atoms. The failures in the LSDA to accurately describe the local correlations in the transition-metal oxides are associated intimately with the local moments.[20] As will be discussed, our calculations demonstrate that the local moments of Fe^{2+} become diminishingly small as pressure increases. Thus we expect the static high-pressure phase of FeO to be metallic, in agreement with band theory. The ratio U/W, where U is the Coulomb repulsion parameter and W is the bandwidth, is a measure of the importance of correlations.[20] At high pressure U/W decreases because W increases, and correlations become less important.

II. METHOD OF CALCULATIONS

We use a general potential version of the LAPW method of Andersen[21] as implemented by Wei and Krakauer[22] to solve the Kohn-Sham[23] equations. This method imposes no shape approximations to the potentials and charge densities. We use the Hedin-Lundqvist exchange-correlation potential for the many-body interactions between electrons,[24] and use spin-scaling from Von Barth and Hedin.[25]

The level of convergence for the calculated total energies is determined primarily by the number of LAPW basis functions used (controlled by the parameter RK-max) and by the **k**-point sampling used for the Brillioun zone integrations. The radii of the atomic muffin tins are $R_{Fe} = 1.8$ and $R_{Oxy} = 1.5$ bohrs for all our calculations, except where noted otherwise. We use $R_{Fe} = 1.645$ and $R_{Fe} = 1.371$ bohrs for the $B1$ NM (and strained calculations) at $V = 9/AA^3$, and correct for the different muffin tin radii used at this volume by calculating the difference in energy at $V = 11/AA^3$ when these two pairs of muffin tin radii are used. For the NM and FM calculations, we use two energy windows where the upper valence window contains the O $2p$ and Fe $3d$ states, and the lower semicore window contains the O $2s$ and Fe $3p$ states. We treat core states fully relativistically and semicore states

semirelativistically which implies in the latter case that spin-orbit coupling, which has negligible effect on total energies for these states, is ignored. Special **k**-point sampling is used[26] with the mesh divisions for the unstrained lattice generated in a cubic supercell (in reciprocal lattice space), and then folded back into the original unit cell. This approach ensures that the correct symmetry is represented; the same **k**-point sampling is used for the rhombohedral lattice whether or not a nonzero strain is applied. We use 19 (6) **k** points in the valence (semicore) window for the $B1$ NM and FM calculations, and 84 (10) **k** points for the $B2$ NM and FM calculations. The $RKmax$ parameter is 8.5 for the $B1$ and $B2$ (NM and FM) calculations, which implies, for example, that 174–194 (depending on the **k** point in question) LAPW basis functions are used at 9 Å^3 ($R_{\mathrm{Fe}} = 1.8$, $R_{\mathrm{Oxy}} = 1.5$) and 424–450 at 21 Å^3. We made numerous tests to ensure that all our results are well converged. In general the energies calculated for the NM and FM spin phases (both $B1$ and $B2$ structures) are converged to better than 1 mRyd. At the smaller cell volumes ($V \leq 12$ Å^3) the convergence with respect to these parameters is to within approximately 2 mRyd.

Great care is required to compare energies between different crystal structures. We obtain the energies of the undistorted AFM $B1$ phase by finding the energy differences between the AFM and FM cases, using four atoms per unit cell for each, and at reduced convergence with respect to $RKmax$ and **k** points than the earlier well-converged two-atom cell calculations. These differences in energy are then added to the well-converged FM energies to represent the AFM energies. We follow this procedure in order to reduce the required computer time for the AFM calculations. Not only is the AFM unit cell twice as large as that usually required for the NM or FM cells, the AFM calculations are more difficult to converge to self-consistency. This is probably due to the presence of more than one energy minimum in spin space. Our AFM calculations are converged to much better than 0.1 mRyd with respect to self-consistency at a particular $RKmax$ and **k**-point sampling. Test runs were performed to ensure that the energy differences between the FM and AFM cases are well converged with respect to further changes in $RKmax$ and in the number of **k** points. In general the energy differences between the AFM and FM configurations are made with $RKmax$=8.0, rather than 8.5, and with 49 **k** points (four atoms per cell) in the irreducible Brillioun zone. This number of **k** points provides convergence to within about 1 mRyd for either the AFM or FM energies alone. The $RKmax$ value of 8.0 provides $\sim 400 - 600$ basis functions in the four-atom cell, typically about 5 mRyd from convergence for the AFM or FM energies alone. We emphasize, however, that the AFM total energies are referenced to the well-converged FM energies by small differences between the FM and AFM cases; these differences are found using the same program (LAPW+LO described below) and with identical **k**-point sampling and $RKmax$ parameters at each volume for the FM and AFM phases.

For both the AFM calculations, and the FM calculations which referenced the AFM energies to the converged FM results, we use an extension to the LAPW method (LAPW+LO) which (1) adds specially constructed local orbitals to the basis in order to eliminate problems with poorly converged core states that can occur under some circumstances, (2) decreases orthogonality errors, and (3) increases variational freedom.[27] We found LAPW+LO convenient because it has sufficient variational freedom to treat both valence and semicore states accurately with one energy window. Furthermore, energies obtained with LAPW+LO are extremely insensitive to the energy parameters.[27]

Total energies at different rhombohedral strains are obtained by finding the difference between the unstrained and the strained energies at each volume. We use sufficient **k** points and basis functions to ensure that this energy difference is converged to about 1 mRyd, and again, emphasize that several tests were performed to ensure convergence. At a given volume we reference all strained calculations to the unstrained case using identical $RKmax$ values and **k** points; the reciprocal lattice coordinates of the **k** points do not change as strain is varied. For example, when calculating the energies of the AFM rhombohedral strained structures, we use 15 **k** points and $RKmax$=7.5 (number of basis functions $\sim 450 - 600$ with a four-atom unit cell) for all the volumes greater than 13 Å^3. At $V = 13$ Å^3, we used 49 **k** points and $RKmax$=8.0 ($\sim$ 480 basis functions). For volumes of 9 and 11 Å^3 we use the two-window LAPW calculation, with two, rather than four, atoms per unit cell since the local moments were zero, and use 5 (semicore) and 30 (valence) **k** points, with $RKmax$=8.5 ($\sim$ 250 basis functions) in both windows.

The rhombohedral strained lattice is obtained by transforming each vector **a** of the original cubic lattice to **a′** by the volume conserving tensor $\underline{G}$ defined by

$$\underline{G} = \begin{bmatrix} 1+g & g & g \\ g & 1+g & g \\ g & g & 1+g \end{bmatrix} (1+3g)^{-\frac{1}{3}}. \quad (1)$$

The rhombohedral angle α is given in terms of the displacement g by

$$\alpha = \cos^{-1}\left[\frac{1}{2}\left(\frac{1+8g+12g^2}{1+4g+6g^2}\right)\right]. \quad (2)$$

III. RESULTS

A. Effects of pressure on the magnetic moments

An important result of our study is the observation that the local moments decrease with decreasing volume (increasing pressure). The volume dependence of the magnetic moments is illustrated in Fig. 1, which shows the net moment in a single FeO cell for the $B1$ FM and AFM, and $B2$ FM phases. Also shown are the AFM moments for the stable strained lattice (discussed in the next section). The FM moments are dominated by contributions from the Fe muffin tins, but unlike the AFM moments, have minor amounts ($\sim$ 7% each) coming

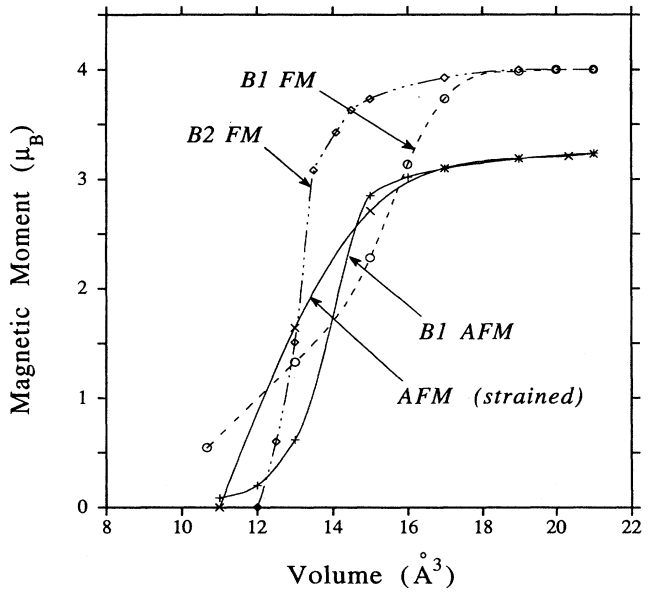

FIG. 1. The volume (pressure) dependence of spin moments for different phases of FeO.

from the oxygen muffin tins and the interstitial charge. We emphasize that a decrease is observed in the local moments as volume is decreased for all the magnetic phases we investigated—$B1$ FM and AFM, $B2$ FM and strained (rhombohedral) AFM. By volumes in the range 11–12 Å^3, which correspond to pressures of about 150–180 GPa, virtually all the local moments are gone. This volume dependence of the local moments is significant because if problems in the LSDA description of FeO at zero pressure are closely related to the magnetic moments, then we expect accurate energies from the LSDA at high pressure.

We find the magnetic moments for the AFM phase to be $3.22\mu_B$ at the experimental primitive cell volume of 20.35 Å^3, and $3.16\mu_B$ at the calculated undistorted $B1$ AFM zero-pressure volume (18.52 Å^3). The AFM moments are defined to be the spin moments within the iron muffin tins, so that a small variation in the calculated moments is seen as the Fe muffin tin radii R_{Fe} are changed. For instance, at $V = 20.35$ Å^3 we increased R_{Fe} from 1.8 to 2.029 49 a.u., the maximum R_{Fe} allowable at this volume since the R_{Oxy} were also increased from 1.50 a.u., and found that the magnetic moment increases to $3.34\mu_B$. We find good agreement with the experimental magnetic moment for FeO of $3.32\mu_B$.[28] Other LSDA calculations, using augmented spherical waves[29] (ASW) and the linear combination of atomic orbitals[30] (LCAO) methods, respectively, have produced values of 3.43 and $3.63\mu_B$ for the AFM magnetic moment at the experimental volume. The small differences between our calculated moments and the ASW results are likely due to the different sizes of atomic spheres used in defining the moments.[29] The difference between our calculated moments and those from the LCAO technique are less obvious, but could be due to differences in basis sets or **k** points. Generalized gradient approximation (GGA) calculations at the experimental volume, using the LCAO method,[30] produced only a slightly lower moment of 3.55, compared to $3.63\mu_B$. In any case, our calculations demonstrate that the magnetic moments calculated for FeO under the LSDA are compatible with experiment, in contrast to the conclusions of Leung, Chan, and Harmon[30] who state that both the LSDA and the GGA inadequately describe the magnetic moments of the three monoxides FeO, CoO, and NiO.

B. Total energies, effects of strain, and equation of state

Results for the calculated energies of FeO over the range of volumes 9.0–21.0 Å^3 and for the different structural and magnetic phases are shown in Fig. 2. For the undistorted $B1$ phase we find very little difference between energies calculated for FM and AFM spin ordering, and find the energies of these two magnetic phases approximately equal at the minimum. At both lower and higher volumes from the minimum, the energy of the unstrained AFM $B1$ phase increases slightly more rapidly than does that of the $B1$ FM phase, although the difference between the $B1$ FM and unstrained AFM phases are reduced at very small volumes.

When rhombohedral strains are applied to the $B1$ structure, we find the stable lattice at each volume to be at nonzero strain for both NM and AFM spin ordering. As pressure increases, both the strain and the change in

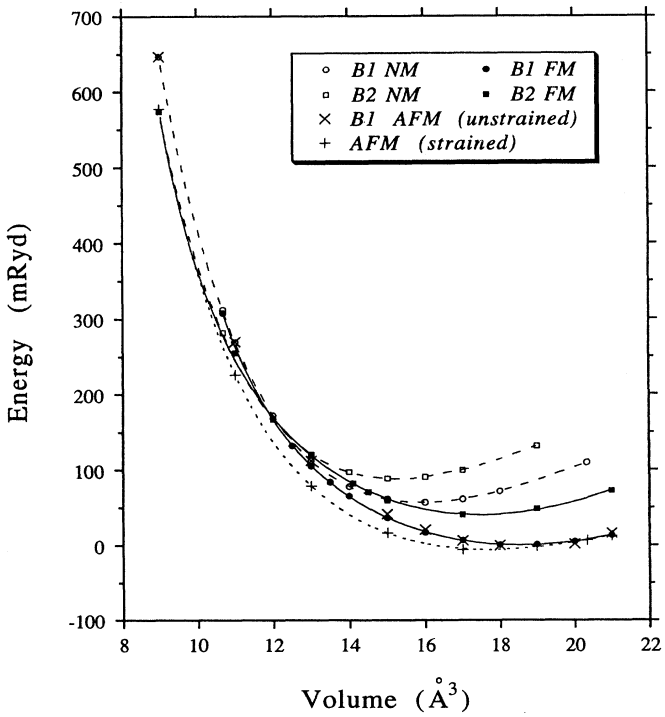

FIG. 2. Total energies for different structural and magnetic phases of FeO. The AFM (strained) curve is for rhombohedral distortion to the $B1$ AFM phase, and shows the energies which have been minimized by straining.

energy associated with the strain where the energy minimum occurs, increase. We illustrate the volume and the strain dependence of the energies for the distorted AFM and NM phases in Fig. 3. The total energies shown in Fig. 2 for the AFM strained case are the $B1$ AFM values corrected by difference in energy required to stabilize the lattice with respect to the rhombohedral strains (Fig. 3).

We investigated the effects of a rhombohedral strain at $V = 20.34$ Å^3, which is near the experimental volume, for both the NM and AFM phases. At this volume the calculated AFM minimum is at a strain of $g = 0.045$ ($\alpha = 54.6°$), and is closer to measured value of $\alpha = 59.5°$ for nonstoichiometric FeO, than is the NM case, which has a minimum in energy at $g = 0.09$ ($\alpha = 49.8°$). Stoichiometry is known to affect the magnitude of α at ambient pressure.[4] Increasing x in Fe_xO causes α to decrease. A linear extrapolation of the data[4] between $x = 0.96$ and 0.97 to $x = 1.0$ gives $\alpha = 58.5°$ for stoichiometric FeO. There is a much stronger dependence of α on stoichiometry for x in the range 0.96–0.97, than found for the range 0.94–0.96. It is possible that increasing x beyond 0.97 results in an even stronger dependence of α on x than for 0.96–0.97, in which case a linear extrapolation of x from 0.97 to 1.0 would significantly overestimate α at $x = 1$. Thus we find that the LSDA gives qualitative agreement with experiment in that a nonzero strained ground state is obtained, and find reasonable quantitative agreement for the strain required to minimize the energy at this volume for which significant moments are present. We also find that the stable phase is at nonzero strain whether or not local moments are present. The spin polarized calculations give improved agreement with the best experimental evidence as to the magnitude of the required strain.

An experimental approximation of the pressure (or volume) dependence of α can be made by assuming that the split (111) line and the (200) line given by Yagi, Suzuki, and Akimota[7] represent the (003), (101), and (102) diffraction lines of a rhombohedral cell. We emphasize that this is only an approximation and note that the diffraction data of Yagi, Suzuki, and Akimoto give a large uncertainty in the calculated cell volume if the cell is constrained to be part of a rhombohedral lattice above 30 GPa. We estimated α as a function of cell volume from the experimental data with a least squares method using the above assumptions regarding the (111) and (200) diffractions and compared with our LAPW results in Fig. 4. The smallest experimental estimate for volume shown in figure is 120 GPa. Very good agreement between LAPW and this estimate of the volume dependence of α from experiment is found for the range of available data, which indicates that interpreting the high-pressure data in terms of rhombohedral structure without major distortions to a lower symmetry is reasonable.

We fit the calculated energies for the structural and magnetic phases to the cell volumes using the Birch equation[31] to determine the zero pressure lattice parameter a, the bulk modulus K, and the pressure derivative of the bulk modulus K'. Results for the $B1$ NM, FM, and AFM phases, and for the strained $B1$ AFM phase, are summarized in Table I for different orders of Birch fits. The relationships between cell volumes (primitive) and pressure obtained from fourth-order Birch fits of the different phases are illustrated in Fig. 5. The energy minimum is at $a = 4.136$ Å for the strained AFM phase, although a found for the $B1$ FM and $B1$ AFM phases are in better agreement with the experimental value of $a = 4.334$ Å.[32] All the magnetic phases have larger lattice parameters in comparison to the NM case (Table I), but all are still less than the experimental value. The lattice parameters calculated for the $B1$ phases are 3% (FM and undistorted AFM), 4.5% (distorted AFM), and 8% (NM) lower than estimated for stoichiometric FeO from experimental data.

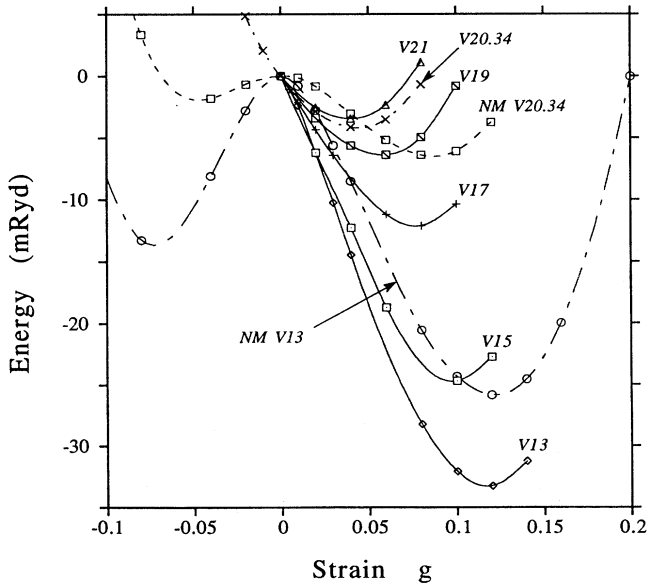

FIG. 3. Volume dependence of strain angle and depth of energy well to obtain energy minimization with respect to rhombohedral strains. Two NM and six AFM volumes are illustrated.

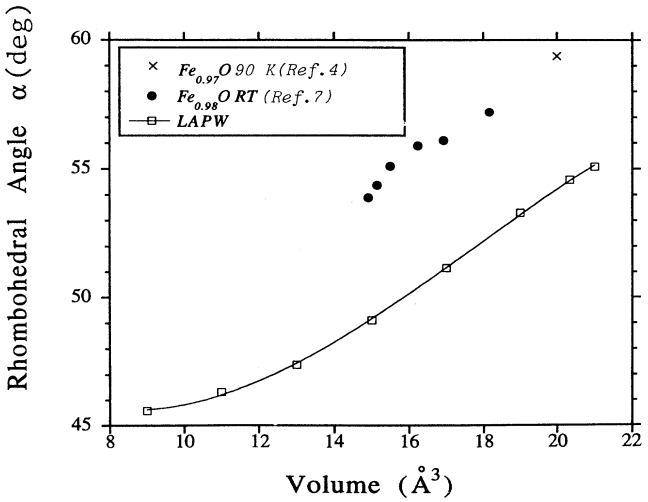

FIG. 4. Comparison of the volume dependence of strain angle α between estimates from high pressure experiments and LAPW calculations.

TABLE I. FeO equation of state parameters and magnetic moment at 0 GPa, calculated with $V = 11 - 21$ Å^3.

	$B1$ NM	$B1$ FM	$B1$ AFM	AFM Strained	Experiment[a]
Second-order fit					
a (Å)	4.002	4.189	4.200	4.135	
K (GPa)	318	169	162	184	
K'	4.0	4.0	4.0	4.0	
rms error (mRy)	1.76	1.80	2.35	0.91	
Third-order fit					
a (Å)	3.996	4.196	4.192	4.136	
K (GPa)	300	151	185	173	
K'	4.6	4.4	3.5	4.3	
rms error (mRy)	0.16	1.52	2.00	0.66	
Fourth-order fit					
a (Å)	3.995	4.204	4.204	4.136	4.334[b]
K (GPa)	303	195	237	173	142-180[b,c]
K'	4.7	1.1	0.3	4.2	4.9[c]
rms error (mRy)	0.06	0.27	0.74	0.66	
μ_B		4.00	3.22	3.23	3.32[d]

[a] The order of fit does not apply to experimental value.
[b] C. A. McCammon and L. Liu, Phys. Chem. Miner. 10, 106 (1984).
[c] I. Jackson, S. K. Khanna, A. Revcolevschi, and J. Berthon, J. Geophys. Res. **95**, 21671 (1990).
[d] W. L. Roth, Phys. Rev. **110**, 1333 (1958).

There is a rather wide range of 142–180 GPa in experimental values reported for the bulk modulus (adiabatic) K_S of nonstoichiometric Fe_xO,[32,33] making comparison with our theoretical results difficult. The range in the data seems too large to attribute to stoichiometric differences of $0.90 \leq x \leq 0.98$ in specimens. Reasons for these variations in the data are the subject of some controversy. While no obvious relationship between x and K_S has been identified, there is evidence that very near $x = 1$, a relatively strong increase in K_S with increasing x occurs.[32,33] Most estimates from extrapolations of experimental data are that K_S lies within 174–183 GPa for $x = 1$.[32–34] These estimates are in agreement with the one datum $K_S = 174$ GPa for which $x = 0.98$.[35] All other data were obtained with specimens for which $x < 0.95$. Alternative conclusions have been made to suggest that K_S for stoichiometric FeO is considerably lower than 174 GPa and lies nearer 155 GPa.[2]

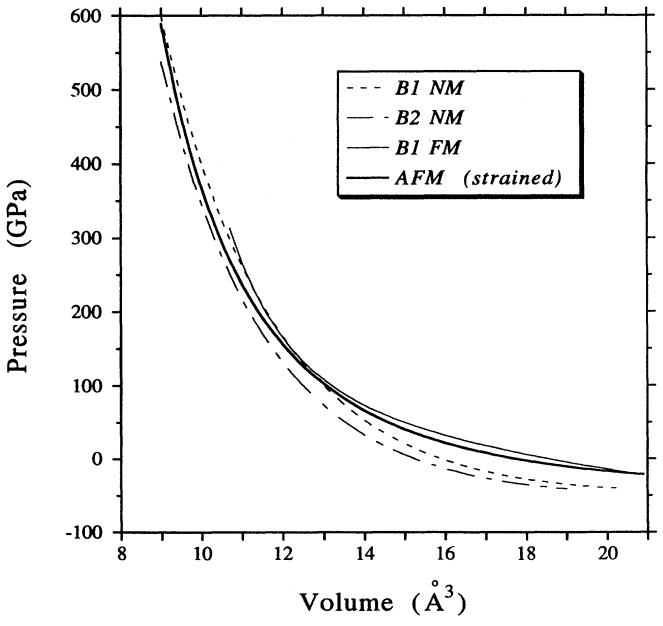

FIG. 5. Equation of state for different phases of FeO. Volume is for primitive cell.

Given the uncertainty in the experimental values for the bulk modulus of FeO discussed above, the calculated values shown in Table I for the magnetic phases are quite reasonable. The small corrections ($\sim 1\%$) to bring the measured adiabatic bulk modulus K_S at ambient conditions to zero temperature can be neglected when comparing our results with experiment. The K for the NM case is significantly larger than experiment, whereas the K from the magnetic phases are generally within, or near to, the experimental range. It is noteworthy that for a third- (fourth-) order Birch fit our strained AFM equation of state gives values for $K = 173$ (173) GPa and $K' = 4.3$ (4.2) at the calculated zero-pressure volume, which are in excellent agreement with experiment. However, the zero pressure experimental volume (20.35 Å^3) corresponds to -18 GPa in our calculated equation of state. We find $K = 92$ GPa (fourth-order Birch fit) at the experimental volume, which is considerably lower than the range in K estimated from experiment.

We find that the FM and AFM equaton of state parameters (except for a) are quite sensitive to the order of fit used. Apparently the relatively flat energy curves

of the magnetic phases hinder an unambiguous mathematical description of these higher-order derivatives (see especially the variation in K' for the $B1$ FM and AFM in Table I). The fits for strained AFM FeO are stable with respect to the order. We also note that the rms errors between the calculated points and the fits are larger for the magnetic phases than for the NM phase, and was also found to be the case when comparing the Birch fits of the $B2$ FM and NM phases.

C. $B1$-$B2$ phase transitions

By comparing the free energies of the $B1$ and $B2$ FM phases, we find a $B1$ (magnetic) to $B2$ (nonmagnetic) transition at 161 GPa. The unit cell decreases in volume across this transition from 12.045 to 11.527 Å^3, or by about 4%. At 11.527 Å^3 the magnetic moment of the $B2$ structure is zero (Fig. 1). We find a similar 4% decrease in volume for a phase transition from the $B1$ unstrained AFM phase to the $B2$ FM phase at 130 GPa. It has been suspected for some time that the $B2$ phase is the stable phase for FeO at high pressure. However, since it is the strained $B1$ AFM lattice which is stable to pressures well beyond 160 GPa, the calculated $B1$ to $B2$ transition pressures of 130 or 160 GPa are not pertinent. We find, however, that at pressures near 500 GPa the $B2$ structure does, indeed, become more stable than the strained $B1$ structure (Fig. 2), and a likely transition to the $B2$ phase is discussed further in the next section.

It seems that a first-order phase transition, from a magnetic to nonmagnetic phase, should be observed around the range in volumes where the magnetic moments decrease rapidly. The relatively large rms errors found for the magnetic phases (Table I) when applying the third- and fourth-order Birch fits to the energy-volume results suggest something other than pure hydrostatic compression contributes to the calculated energy-volume relationship. We carefully investigated this possibility for both the $B1$ and $B2$ FM phases. We find no evidence for a first-order transition for the $B1$ FM phase. We plot the $B1$ energies in Fig. 6, which shows that the FM curve smoothly joins the NM curve around 12 Å^3. We find with the $B2$ phase clear signs of a first-order transition where the FM curve approaches the NM curve (Fig. 7). The $B2$ FM energies are seen to deviate from the Birch fit at the volumes 13–15 Å^3 where the local moments decrease rapidly with increasing pressure. Since the moments (FM) for the $B1$ structure tend to decrease more gradually with increasing pressure than for the $B2$ structure, a first-order transition may occur in the $B1$ phase also, but this cannot be determined conclusively with our sampling of volumes. We note that in the volume range where this first-order transition is observed in the $B2$ structure, it is the $B1$ structure that is the stable phase.

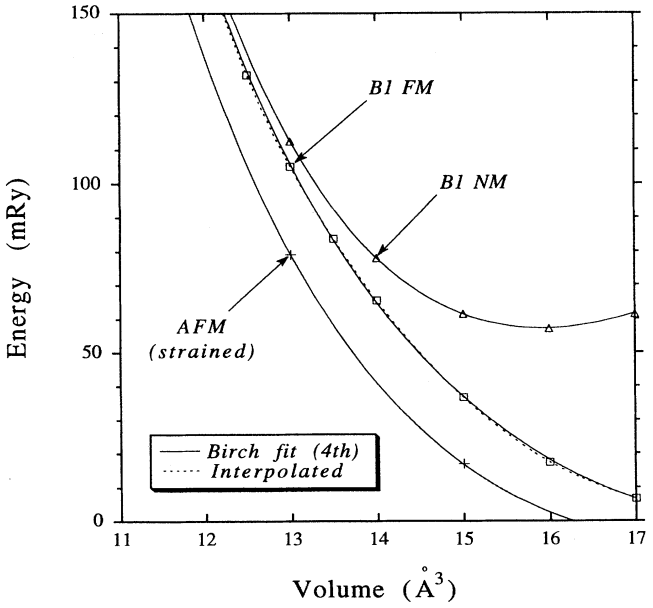

FIG. 6. $B1$ structure energies near where the FM and NM curves converge. No first-order transition from the FM to NM phases is resolvable.

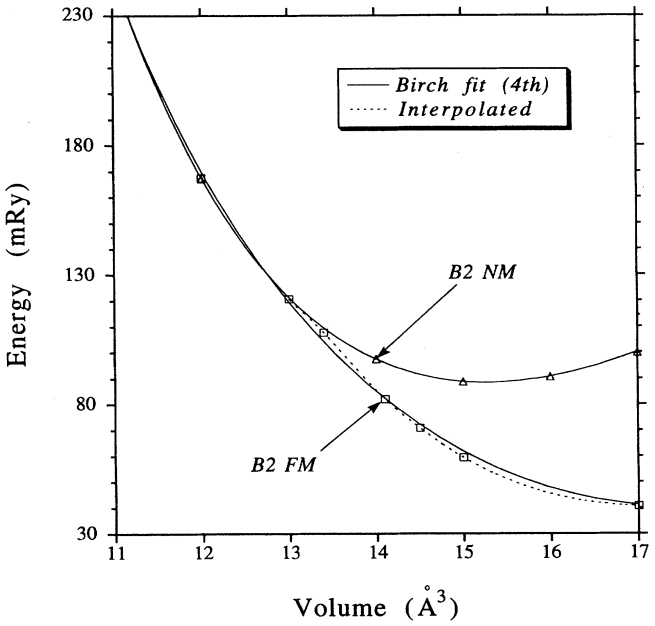

FIG. 7. $B2$ structure energies near where the FM and FM curves converge. An apparent first-order transition between these two phases occurs. Note the deviation from the Birch fit which the $B2$ FM phase makes from 13 to 15 Å^3.

IV. DISCUSSION

It is widely accepted that the reason for the differences between band calculations and experiments in the transition monoxides is the inability of the LSDA to accurately describe strongly correlated systems. The fact that FeO loses its local moments at high pressure implies that it transforms from an antiferromagnetic, insulating material to a nonmagnetic, metallic material.[20] Since a

failure of the LSDA to accurately describe details of a material's insulating phase does not rule out its accurate application to the metallic phase,[36] we expect the LSDA to provide an accurate description of the properties of FeO at high pressure. While we have emphasized the expectation that the LSDA provides accurate information on the properties of FeO at high pressures where the local moments and magnetic energies are negligible, we also find resonable agreement with experiment for several calculated properties of FeO at, or near, the ambient volume where the local moments are large. The magnitude of the zero-pressure moments and of the equation of state parameters, K and K', the AFM nonzero [111] strain as the stable configuration relative to $B1$, and the pressure dependence of the strain angle at relatively low pressures all show good agreement with experiment. It seems that the total energies calculated by the LSDA are reasonably accurate even with the presence of local moments.

The lattice parameter of the calculated ground state (strained AFM) is underestimated by about 4.5% when compared with experiment, which is large relative to the LSDA results for many materials.[37] As emphasized by Leung, Chan, and Harmon,[30] systematic errors in the LSDA tend to underestimate the lattice parameter of many materials. For instance, using LSDA, the cell parameters are underestimated by 3.5% and 2.5%, respectively, for Fe and NiO.[38,30] The smaller cell parameter found for FeO by the LSDA band calculations may well result from the fact that FeO is incorrectly described as a metal by the theory. But the relationship between details of the electronic band structure and the total energies is complex. A formalism which improves the electron band structure does not necessarily improve other properties, and visa versa. For instance, efforts to obtain a better exchange-correlation functional form using GGa's have brought significantly better convergence between experiment and theory for the lattice parameter of NiO, but do not significantly improve the poor description which the LSDA obtains for the band structure and the magnetic moments of NiO at ambient volume.[30]

At sufficiently high pressures and room temperature many $B1$ monoxides are believed to undergo a transition from the $B1$ to the close-packed $B2$ structure. This type of transition has been observed in the larger of the monoxides, i.e., BaO, SrO, CaO, and EuO.[39] While there are no conclusive data requiring a $B1$-$B2$ transition for monoxides with smaller cations, Kawai and Mochizuki[40] suggest such a transition to explain the sudden drop in the resistivity of NiO observed near 100 GPa at room temperature. Shock results certainly allow for a $B1$ to $B2$ transition in FeO at high temperature, but no discontinuous change in volume has been observed experimentally in diamond cell experiments at room temperature and to pressures of 220 GPa.[45] Our results show that a simple rhombohedral distortion along [111] lowers the energy sufficiently to prevent the $B2$ phase from being the more stable phase for pressures up to about 500 GPa. If the high-pressure, high-temperature metallic phase[12] is indeed a $B2$ structure, our results indicate why no transition has been observed in static experiments. Specifically, we find that above 520 GPa, when fourth-order Birch fits are used in comparing the energies of two structures, the $B2$ phase is more stable than the strained $B1$ structure, and a transition to the $B2$ lattice occurs with volume changing from 9.27 to 9.09 Å^3 ($\sim$ 2%). It is of interest that LAPW calculations done by Mehl and Cohen[41] indicate a $B1$-$B2$ transition also occurs at about 520 GPa for MgO, and that the volume reduces by about 4% across this transition.

The exact pressure of our predicted transition for FeO varies somewhat according to the fit used. For example, when third-order Birch fits are used to represent the energies for each phase, we find the transition pressure to be 480 GPa, and the volume changes from 9.37 to 9.27 Å^3 ($\sim$ 1%). We must mention that even when the uncertainties associated with our convergence are considered, our calculations predict a transition to the $B2$ structure occurs near 500 GPa. If the calculated energy of the strained structure at 9 Å^3 is changed by ± 2 mRy, our maximum estimated uncertainty due to convergence, the transition pressure with a fourth-order fit ranges from 501 (+2 mRy) to 536 (−2 mRy) GPa.

The decrease in the energy of the strained $B1$ structure, relative to the unstrained $B1$ lattice, is related to the fact that the rhombohedral angle α is less than 60^o for the stable lattice at a given pressure. Our calculations are for stoichiometric FeO, i.e., $x = 1$ in Fe_xO. Nonstoichiometry tends to increase α, relative to stoichiometric FeO; at a given pressure we do not expect as large a decrease in strained energy for nonstoichiometric FeO as for when $x = 1$. It is possible that future experiments will find a transition pressure somewhat lower than 500 GPa since x greater than about 0.98 in Fe_xO is not easily attainable.

All our calculations are at zero temperature. We believe that some sense of the temperature dependence of the transition to the $B2$ structure can be found by associating E_S, the energy due to strain at each volume (see Fig. 3), with temperature. At zero temperature the strained lattice energy is lowered by E_S relative to the unstrained $B1$ lattice, and this prevents a $B2$ transition at pressures lower than 520 GPa. However, temperatures on the order of E_S (or some fraction thereof) may effectively eliminate the strain found in the zero-temperature lattice, and, therefore, allow the $B2$ phase to be stable relative to $B1$ at pressures much lower than 520 GPa. For instance, we find the $B2$ phase stable relative to the unstrained $B1$ AFM phase at zero temperature and pressures greater than 130 GPa. The volume at 130 GPa is a little larger than 12 Å^3 (Fig. 5), and E_S is about 35 mRy (corresponding to about 5500 K). Thus, we expect that at 130 GPa as temperature increases there comes a point (5500 K, or less) at which the strain diminishes to the extent that a transition to $B2$ can occur. As pressure increases, E_S also increases, implying that the temperature required to remove the strain also increases; the $B1$-$B2$ phase boundary has a positive slope in P, T space. We illustrate this proposed phase relationship between $B1$ and $B2$ in Fig. 8 with a sketch (short-dashed line). For our discussion we assume the AFM phase is synonomous with the $B1$ structure (which includes rhombohedral strains), and assume the metallic

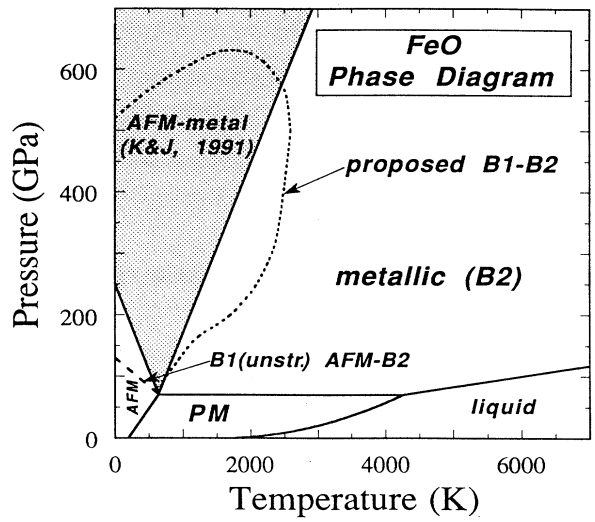

FIG. 8. Phase diagram for FeO [after Knittle and Jeanloz (KJ) (Ref. 12)] showing a sketch of our proposed temperature dependence of the strained $B1$-$B2$ transition (short-dashed lines). Solid lines are the phase boundaries indicated by KJ; the shaded region is the range of uncertainty suggested by KJ for an AFM to metallic transition (assumed $B1$ to $B2$ here). The long-dashed line connects the zero-temperature $B1$ (unstrained) AFM to $B2$ transition (our calculation) with the triple point at around 650 K and 70 GPa given by KJ.

phase has the $B2$ structure. In Fig. 8 we start from the triple point at 650 K and 70 GPa,[12] and we then indicate a stronger temperature dependence for the boundary separating the $B1$ and $B2$ phases than suggested by Knittle and Jeanloz, since E_S increases somewhat more rapidly with pressure than indicated by the right-hand side of the AFM-metallic boundary range (shaded region of Fig. 8). For example $E_S = 43.6$ mRy (6800 K) at 11 Å^3 (237 GPa), compared to 33.3 mRy (5200 K) at 13 Å^3 (103 GPa). Eventually this phase boundary must loop around in P,T space to intersect the zero-temperature axis near 520 GPa, the point at which we calculate a transition.

We cannot discount the possibility that at high pressure the rhombohedral lattice is unstable to other distortions, which further decrease the energy and put the lattice into a lower symmetry. Yagi *et al.*[7] mention that distortions from the rhombohedral cell may provide an explanation for the poor fit of the x-ray data to a hexagonal (rhombohedral) cell at pressures greater than about 30 GPa. Diffractions similar to those reported by Yagi *et al.*[7] have been observed by others in experiments up to 70 GPa (Ref. 44) and 220 GPa.[45] These data all indicate further distortions from rhombohedral symmetry at high pressure are possible. What is not certain from the data is whether or not a distortion of the rhombohedral cell to lower symmetry occurs in response to shear stresses in the experiments. We predict, in the absence of further significant distortions from the rhombohedral phase, that FeO undergoes a transition to the $B2$ structure at 520 GPa and zero temperature, and that at this pressure both phases are metallic.

In addition to the possibility that a structure with lower than rhombohedral symmetry occurs before the transition to $B2$, it may also be that internal displacements, i.e., displacements of the oxygen ion relative to Fe within the cell, occur. The effect would be to lower the energy of the strained cell to the extent that a transition to $B2$ cannot occur or takes place at even higher pressure than 500 GPa. We did investigate the possibility for the strained $B1$ structure by displacing the oxygen ion from their positions at the center of the unit (nonprimitive) cell. We first displaced each oxygen in the same direction along the [111] axis (IR-type displacements). A second series of calculations were done changing the direction of the displacement of every other oxygen along a given [111] axis (Raman-type displacements). In this latter case the oxygens are moving towards Fe^{2+} ions of a given spin, and away from the ions of the opposite spin. Results of these calculations are illustrated in Fig. 9 at different rhombohedral strains and for several different displacements of the oxygen ions. We find a distinct energy increase for any displacement of the oxygen away from the cell center for both types of displacements we investigated, and therefore, discount the possibility that these internal cell rearrangements can produce a minimum in energy at nonzero displacement.

We note that by extrapolating to large volumes, corresponding to negative pressure, the rhombohedral strain diminishes to zero and then, presumably, is negative. A negative strain corresponds to compression of one body diagonal, and symmetric extension of the other three, which implies an angle α greater than 60°. At ambient pressure, when MnO and NiO cross their Néel temperatures, 160 and 470 K,[3,42] respectively, α becomes greater than 60°. Apparently the phase line between the cubic

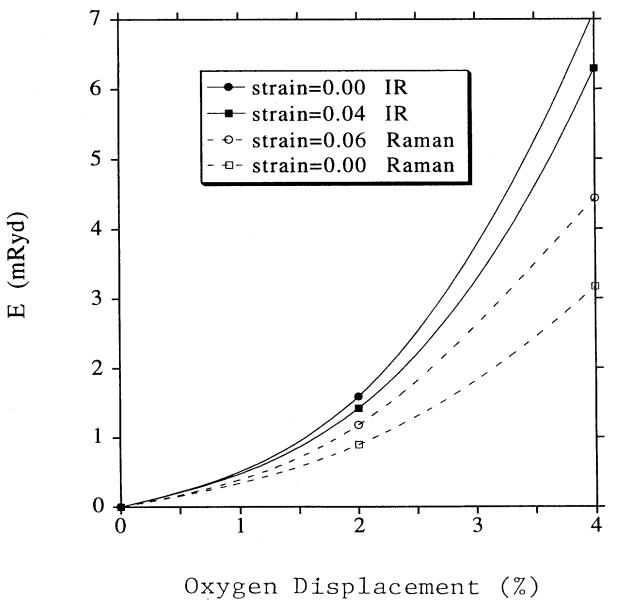

FIG. 9. Strained and unstrained energy variations of the FeO cell as oxygen ions are displaced from the center towards the corner Fe.

(or approximately so) and the AFM rhombohedral structures of both MnO and NiO is shifted upward on the pressure axis relative to that of FeO. By analogy with the behavior of FeO, we suggest that under pressure, α for both MnO and NiO will first approach 60°, i.e., the strain will actually decrease until a cubic structure is obtained. Further pressure will then result in α becoming smaller in these two materials.

Since a strained lattice occurs whether or not local moments are present, the strain cannot be only a consequence of the introduction of moments. In order to gain understanding of the mechanism driving the lattice to strain we performed electronic density of states (DOS) calculations, using the $B1$ NM phase at a cell volume of 13 Å^3, and for strains $g = 0.00$ and 0.12 (Fig. 10). The strain of $g = 0.12$ is near where the minimum in energy is found for this volume. A peak in the DOS at the Fermi energy E_F is generally associated with instabilities in the lattice. We see in Fig. 10 for the unstrained case a peak that is near to, but not at, E_F. Therefore, a high DOS at E_F is not driving this tendency to strain. In Fig. 10 the states in the 1.0–1.4 Ryd range are predominantly Fe 3d, and those in the two peaks near 0.5 Ryd are mostly O 2p. There is a distinct tendency for both Fe 3d and O 2p states to broaden out in the DOS plot as the $B1$ lattice is strained. It appears that when the lattice is strained, hybridization occurs between the Fe 3d and O 2p states, as seen in Fig. 10 around 0.4 Ry below E_F.

Insight in the change in bonding character when strain occurs is gained from charge density difference plots (Fig. 11). These plots show the difference between the self-consistent (LAPW) charge density and the charge density of overlapped spherical Fe^{2+} and O^{2-} ions as in the potential induced breathing (PIB) model.[43] As the lattice is strained, planes (perpendicular to the [111] direction) of nearest-neighbor-like atoms are coming together and nearest-neighbor-unlike atoms are moving

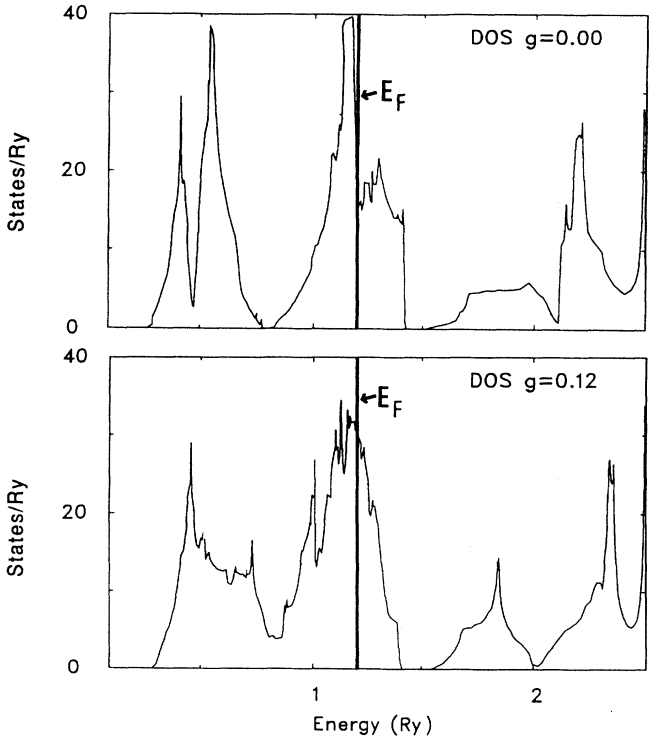

FIG. 10. Density of states for the unstrained and strained $B1$ lattice at a cell volume of 13 Å^3. The strain ($g = 0.12$) is approximately that required to minimize the energy.

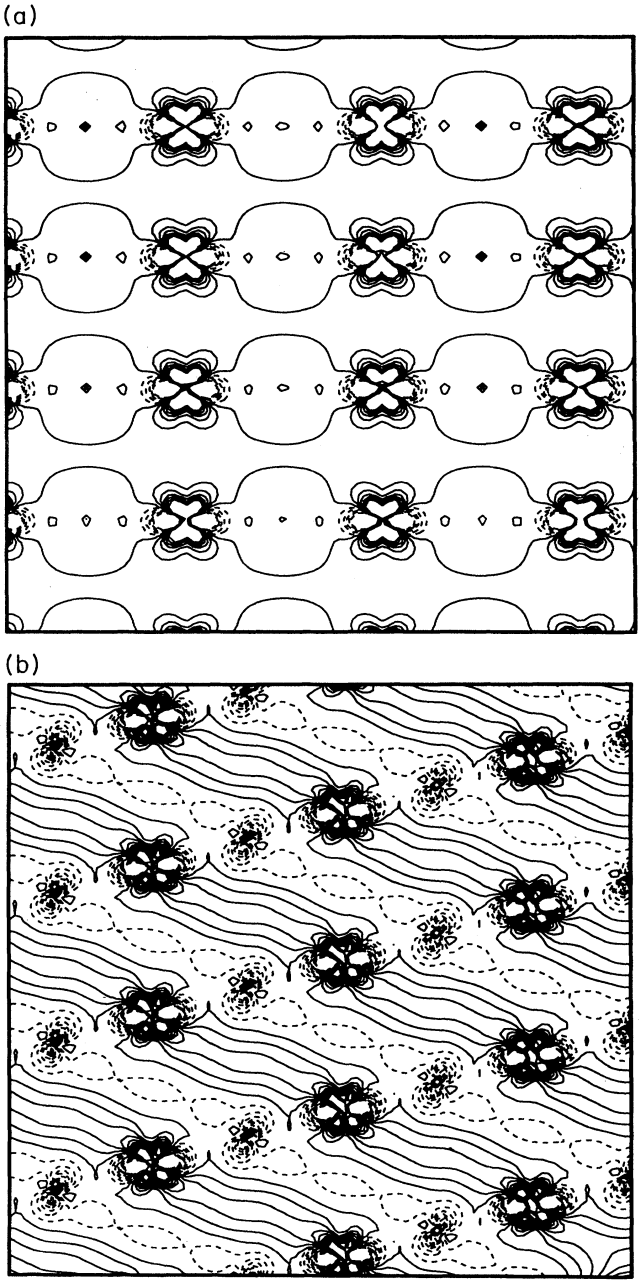

FIG. 11. Electron density difference plot showing the regions where bonding increases between the case for overlapping spherical ions and LAPW calculated densities. Note the increase (solid lines) in Fe-Fe bonding with the strained lattice (b), relative to the unstrained lattice (a). The contour range is −0.1 to 0.1 electrons/bohr^3 at an interval of 0.02. The zero contour is omitted.

apart. The striking feature of Fig. 11 is the increase in Fe-Fe bonding in a given plane perpendicular to the [111] direction at the expense of the bonding between the nearest-neighbor-unlike Fe and O ions. Thus we find a significant rearranging of the bonding in FeO with rhombohedral strains, and a tendency for the metallic cations to form strong covalent-metallic bonds with each other.

We must note that the decrease in local moments with increasing pressure corresponds to a change from a high-spin to a low-spin configuration at high pressure. Thus the chemistry of the Fe^{2+} ion is different at high pressure from that at low pressure, and its relationship to Mg^{2+} in mineral solid solutions such as magnesiowüstite (Mg,Fe)O which appears to be an ideal solution at low pressures may be decidedly changed at high pressure. For instance, immiscibility between Mg-rich and Fe-rich phases may become common at high pressures.

V. CONCLUSIONS

Problems with the LSDA description of the antiferromagnetic transition-metal oxides are generally believed to be associated with strong correlations and local magnetic moments. A marked decrease in magnetic moments of FeO occurs with increasing pressure, and therefore we suggest the LSDA description of FeO should be reasonably accurate at high pressure. We find that the $B1$ structure is unstable to rhombohedral strains whether or not local magnetic moments are present, and that the strain required to stablize the lattice increases with increasing pressure. The good agreement between LSDA calculations and estimates from experiment regarding the volume dependence of α suggests that the high-pressure, low-temperature structure may indeed be interpreted in terms of a rhombohedral structure up to 70 GPa, with only slight distortions to lower symmetry.

The electronic structure and bonding character of the strained lattice show considerable differences from the unstrained $B1$ structure. In particular we find an increase in bonding between nearest Fe ions, at the expense of bonding between Fe and O, as the lattice is strained. We find that the strain lowers the energy of stoichiometric FeO sufficiently to prevent a transition to the $B2$ phase at pressures below 500 GPa. If no other distortions occur in the rhombohedrally strained lattice causing it to go to a lower symmetry, our results may provide the explanation as to why a discontinuous change in volume is observed at 70 GPa in dynamcal studies (shock), but has not been observed up to 220 GPa at room temperature with diamond cell experiments. We predict that a transition of stoichiometric FeO from a rhombohedrally strained $B1$ structure to the $B2$ structure occurs at low temperature near 500 GPa. We suggest from our results that the $B2$ transition can occur at lower pressures with increased temperature, and that the phase boundary between the $B1$ and $B2$ structures has a positive slope in P,T space for pressures in the range of 70 to about 400 GPa.

ACKNOWLEDGMENTS

We thank W. Pickett, R. Hemley, R. Hazen, Y. Fei, E. Knittle, and H. K. Mao for helpful discussions and for providing information from unpublished data. Computations were performed on the Cray 2 and Cray YMP at the National Center for Supercomputing Applications (University of Illinois at Urbana) under the auspices of the National Science Foundation. This research was supported by the Office of Naval Research through Grant No. N00014-92-J-1354 and work at the Naval Research Laboratory (Isaak), by NSF Grant No. EAR91-17280, and by the Geophysical Laboratory (Carnegie Institution of Washington, D.C.).

*Also at Department of Mathematics and Physics, Azusa Pacific University, Azusa, California 91702-7000.

[1] D. J., Stevenson, Science **241**, 611 (1981).
[2] R. M. Hazen and R. Jeanloz, Rev. Geophys. Space Phys. **22**, 37 (1984).
[3] N. C. Tombs and H. P. Rooksby, Nature **165**, 442 (1950).
[4] B. T. M. Willis and H. P. Rooksby, Acta Crystallogr. **6**, 827 (1953).
[5] C. G. Shull, W. A. Strauser, and E. O. Wollan, Phys. Rev. **83**, 333 (1951).
[6] G. T. Zou, H. K. Mao, P. M. Bell, and D. Virgo, Carnegie Inst. Washington Yearb. **79**, 374 (1980).
[7] T. Yagi, T. Suzuki, and S. Akimoto, J. Geophys. Res. **90**, 9784, (1985).
[8] R. Jeanloz and T. J. Ahrens, Geophys. J. R. Astron. Soc. **62**, 505 (1980).
[9] E. Knittle and R. Jeanloz, J. Geophys. Res. **13**, 1541, (1986).
[10] E. Knittle, R. Jeanloz, A. C. Mitchell, and W. J. Nellis, Solid State Commun. **59**, 513, (1986).
[11] T. Yagi, K. Fukuoka, H. Takei, and Y. Syono, Geophys. Res. Lett. **15**, 816 (1988).
[12] E. Knittle and R. Jeanloz, J. Geophys. Res. **96**, 16169 (1991).
[13] D. M. Sherman, J. Geophys. Res. **96**, 14 299 (1991).
[14] A. Navrotsky and P. K. Davies, J. Geophys. Res. **86**, 3689, (1981).
[15] D. Adler, Rev. Mod. Phys. **40**, 714 (1968).
[16] J. B. Goodenough, in *Progress in Solid State Chemistry*, edited by H. Reiss (Pergamon, New York, 1971), Vol. 5.
[17] B. H. Brandow, Adv. Phys. **26**, 651 (1977).
[18] D. M. Sherman, Geophys. Res. Lett. **16**, 515 (1989).
[19] V. I. Anisimov, J. Zaanen, and O. K. Andersen, Phys. Rev. B **44**, 943, (1991).
[20] N. F. Mott, *Metal-Insulator Transition* (Taylor and Francis, London, 1990).
[21] O. K. Andersen, Phys. Rev. B **12**, 3060 (1975).
[22] H. Wei and H. Krakauer, Phys. Rev. Lett. **55**, 1200 (1985).
[23] *Theory of the Inhomogeneous Electron Gas*, edited by S. Lundqvist and N. H. March (Plenum, New York, 1983).
[24] L. Hedin and B. I. Lundqvist, J. Phys. C **4**, 2064, (1971).
[25] U. Von Barth and L. Hedin, J. Phys. C **5**, 1629 (1972).

[26]A. Baldereschi, Phys. Rev. B **7**, 5212 (1973); D. J. Chadi and M. L. Cohen, *ibid.* **8**, 5747 (1973); H. J. Monkhorst and J. D. Pack, *ibid.* **13**, 5188 (1976); **16**, 1748 (1977).
[27]D. Singh, Phys. Rev. B **43**, 6388 (1991).
[28]W. L. Roth, Phys. Rev. **110B**, 1333 (1958); D. Hermann-Ronzaud, P. Burlet, and J. Rossat Mignod, J. Phys. C **11**, 2123 (1978).
[29]K. Terakura, T. Oguchi, A. R. Williams, and J. Kübler, Phys. Rev. B **30**, 4734 (1984).
[30]T. C. Leung, C. T. Chan, and B. N. Harmon, Phys. Rev. B **44**, 2923 (1991).
[31]F. Birch, J. Geophys. Res. **83**, 1257 (1978).
[32]C. A. MaCammon and L. Liu, Phys. Chem. Miner. **10**, 106 (1984).
[33]I. Jackson, S. K. Khanna, A. Revcolevschi, and J. Berthon, J. Geophys. Res. **95**, 21671 (1990).
[34]L. J. Bonzcar and E. K. Graham, J. Geophys. Res. **87**, 1061 (1982); I. Jackson, R. C. Liebermann, and A. E. Ringwood, Phys. Chem. Miner. **3**, 11 (1978).
[35]H. Mitzutani, Y. Hamano, S. Akimoto, and O. Nishizawa, Eos Trans. Am. Geophys. Union **53**, 527 (1972).
[36]W. E. Pickett, H. Krakauer, R. E. Cohen, and D. J. Singh, Science **255**, 46 (1992).
[37]M. J. Mehl, J. E. Osburn, D. A. Papaconstantopoulos, and B. M. Klein, Phys. Rev. B **41**, 10311, (1990); S. R. Chubb, D. A. Papaconstantopoulos, and B. M. Klein, *ibid.* **38**, 12120 (1988).
[38]C. S. Wang, B. M. Klein, and H. Krakauer, Phys. Rev. Lett. **54**, 1852 (1985).
[39]L. G. Liu and W. A. Bassett, *Elements, Oxides, and Silicates* (Oxford University Press, New York, 1986).
[40]N. Kawai and S. Mochizuki, Solid State Commun. **9**, 1393 (1971).
[41]M. J. Mehl and R. E. Cohen, J. Geophys. Res. **93**, 8009 (1988).
[42]H. P. Rooksby, Acta Crystallogr. **1**, 226 (1948).
[43]L. L. Boyer, M. J. Mehl, J. L. Feldman, J. R. Hardy, J. W. Flocken, and C. Y. Fong, Phys. Rev. Lett. **54**, 1940 (1985); M. J. Mehl, R. J. Hemley, and L. L. Boyer, Phys. Rev. B **33**, 8685 (1986); R. E. Cohen, L. L. Boyer, and M. J. Mehl, *ibid.* **35**, 5749 (1987).
[44]Y. Fei (private communication).
[45]H. K. Mao (private communication).